Sensorless Open-Circuit-Fault Diagnosis Method for NPC-based DAB Converter

Song, Chaochao; Sangwongwanich, Ariya; Blaabjerg, Frede

Published in:
I E E E Transactions on Power Electronics

DOI (link to publication from Publisher):
10.1109/TPEL.2024.3409060

Publication date:
2024

Document Version
Accepted author manuscript, peer reviewed version

Sensorless Open-Circuit-Fault Diagnosis Method for NPC-based DAB Converter

Chaochao Song, *Member, IEEE,* Ariya Sangwongwanich, *Member, IEEE,* and Frede Blaabjerg, *Fellow, IEEE*

***Abstract*—Open-circuit fault (OCF) on power switches can cause a severe threat to operation and safety of power electronic converters. In the neutral-point-clamped (NPC)-based dual-active-bridge (DAB) converters, the OCFs will result in an increase in the current stress, DC bias, and capacitor voltage imbalance. In order to address these issues, the faulty switch should be identified so that a fault-tolerant control can be employed to ensure the safe operation of the DAB converter. In existing fault diagnosis (FD) methods, extra voltage and/or current sensors are required, which will increase the hardware costs and volume. This letter proposes an FD method for the NPC-based DAB converters without additional sensors. In the proposed method, the faulty switch can be identified from the average bridge-leg-midpoint (BLM) voltages after blocking certain complementary inner switch (CIS). The average BLM voltage of each bridge leg is detected by an average-value-detecting (AVD) circuit, which is composed of an operational amplifier and passive components. Thus, the proposed FD approach will not increase the costs and volume of the DAB converter significantly. In addition, the proposed FD method also have the features of simple control structure, relatively fast diagnostic speed, and generic application to various modulation strategies. Finally, experimental tests are conducted to validate the effectiveness of the proposed FD method.**

***Index Terms*—Neutral-point-clamped topology, dual-active-bridge converter, open-circuit fault, fault diagnosis.**

I. Introduction

NEUTRAL-point-clamped (NPC)-based dual-active-bridge (DAB) converter can be applied to medium-voltage DC (MVDC) applications due to increased voltage blocking capability and step-up ratio compared to traditional two-level DAB topology [1]–[3]. Fig. 1 shows a typical NPC-based topology called two-three (2/3)-level DAB converter, where a full bridge is applied to the lower-voltage side, and a NPC bridge is used in the higher-voltage side.

An open-circuit fault (OCF) can occur in NPC-based DAB converters due to a failure in pulse generation, gate driver, and packaging and inter-connection of power switch [4]. When an OCF occurs, the voltage and current waveforms becomes asymmetrical, and a DC bias will appear on the inductor current, which will further increase the peak current and cause potential magnetic saturation [4], [5]. In addition, the capacitor voltage balance will be disrupted, resulting in higher voltage stress on certain power devices [3]. In order to avoid these negative issues, a fault-tolerant control strategy should be applied to bring the converter back to a safe operating range [3], [4]. This requires that the faulty switch should be first identified. Post-fault characteristics are used as diagnostic signals for faulty-switch identification. The fault diagnosis (FD) methods for NPC inverters/rectifiers have been widely researched, where the phase currents, pole voltages, DC-link capacitor voltages are generally applied to achieve faulty switch location [6]–[8]. However, when the NPC bridge is used to the DAB converters, the FD methods proposed for NPC inverters/rectifiers are not suitable for the NPC-based DAB converters due to different modulation strategies and switching characteristics. For instance, the inductor current (i.e., i_L in Fig. 1) undergoes periodic variations with a switching cycle instead of a grid cycle as in inverters/rectifiers, and the zero-crossing points of the inductor current are affected by various factors, e.g., voltage and power levels, operation modes, and non-ideal issues like slight DC bias, which makes the current polarity very challenging to be determined under a certain switching state. As a result, the FD methods requiring current polarity identification for inverters/rectifiers, e.g., in [7] and [8], cannot be applied to NPC-based DAB converters. On the other hand, some FD methods have also been developed for the DAB converters. In [9]–[12], the faulty switch is located by using the terminal voltage and/or current of the transformer (i.e., v_{ab}, v_{cd}, and i_L in Fig. 1). Bridge-leg-midpoint (BLM) voltage (e.g., v_{cn} and v_{dn}) is another commonly used fault diagnostic signal [13]–[15]. However, the above FD approaches were proposed based on traditional two-level DAB converter. When applying these methods to the NPC-based DAB converters, the post-fault characteristics of the outer and inner switches in a same upper/lower bridge leg (e.g., S_{21} and S_{22}) are similar, and thus, specific faulty switch cannot be determined. The OCF-related research for multi-level DAB converters is very limited. The post-fault modes and fault-tolerant control strategy was discussed in [16]. Nevertheless, the FD method was not analyzed. An FD method based on average value and duty cycle of the BLM voltages was proposed for the NPC-based DAB converters in [3]. In this method, the two switches with similar post-fault characteristics can be differentiated by the duty cycle of the BLM voltage after a waveform transition. However, four extra voltage sensors are required for measuring the BLM voltages, which will increase the hardware costs and volume. Furthermore, to obtain the voltage value during the faulty interval, multi-sampling points are required in each switching period. Otherwise, the detected average voltage will not change, and the faulty switch cannot be diagnosed. Therefore, a high-performance microcontroller, which can support multi-sampling and corresponding calculations, is needed for the FD method in [3].

Manuscript received March 28, 2024; revised May 13, 2024; accepted May 30, 2024. This work was supported by the research project Reliable Power Electronic based Power Systems (REPEPS) by the Velux Foundations under Award 00016591. (*corresponding author: Chaochao Song*.)

The authors are with AAU Energy, Aalborg University, 9220 Aalborg, Denmark (e-mail: chso@energy.aau.dk, ars@energy.aau.dk, fbl@energy.aau.dk).

Color versions of one or more figures in this article are available at xxxxxxxxxxx

Digital Object Identifier xxxxxxx

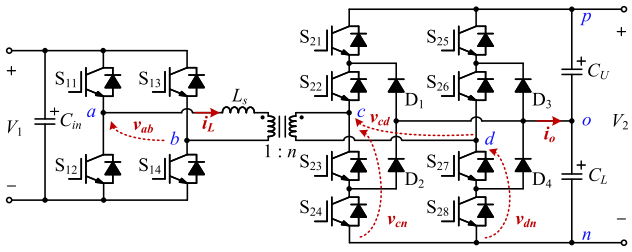

Fig. 1. A two-three (2/3)-level dual-active-bridge (DAB) DC-DC converter.

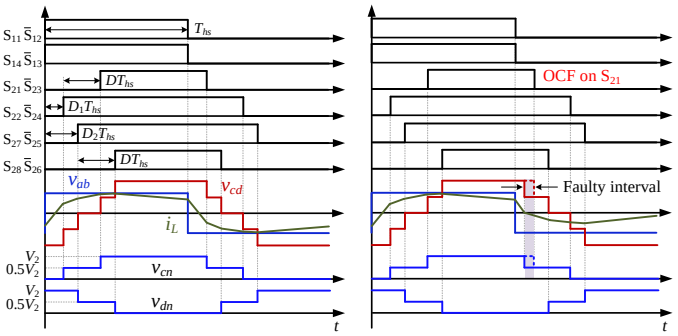

Fig. 2. Multi-phase-shift control strategy for NPC-based DAB: (a) pre-fault waveforms, and (b) post-fault waveforms when an OCF occurs on S_{21}.

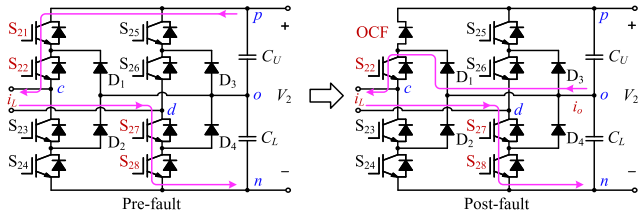

Fig. 3. Current conduction path during the faulty interval when an OCF occurs on S_{21}.

In order to address the above issues, a sensorless FD method is proposed for the NPC-based DAB converters in this letter, which can achieve:

• *certain faulty switch location with simple control structure:* The post-fault conditions of the outer and inner switches can be differentiated by the average midpoint voltage after blocking a certain complementary inner switch (CIS). In addition, only the midpoint voltages are needed to be detected during the entire diagnosis process, which can simplify the FD control structure compared to the prior-art methods which require the combinations of various diagnostic signals;

• *low hardware costs and computation burdens:* The FD process is achieved with an average-value-detecting (AVD) circuit composed of operational amplifier and passive components, and thus, the hardware costs and volume, and computation burdens of the microcontroller can be reduced compared to the sensor-based FD methods;

• *generic application under various modulation strategies:* The proposed FD methods can be applied to the modulation strategies with various degrees of freedom, e.g., single-phase-shift (SPS) control, triple-phase-shift (TPS) control, and five-level control.

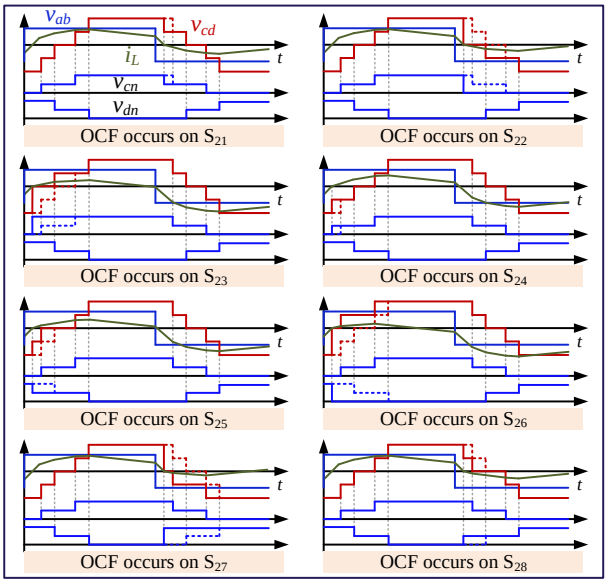

Fig. 4. Post-fault waveforms when an OCF occurs on the NPC bridge.

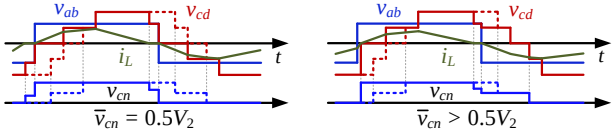

Fig. 5. Post-fault waveforms after the CIS S_{23} is blocked when an OCF occurs on: (a) S_{22}, and (b) S_{21}.

II. Proposed Fault Diagnosis Approach

A. Pre- and Post-fault Characteristics

Fig. 2(a) illustrates a typical multi-phase-shift control strategy, where D_1 and D_2 denote two phase-shift angles, D denotes the duty cycle, and T_{hs} is half of a switching cycle. In pre-fault state, the waveforms of the two voltages v_{ab} and v_{cd} are symmetrical during each switching cycle, and the inductor current is also symmetrical due to

$$\frac{di_L(t)}{dt} = \frac{v_{ab}(t) - v_{cd}(t)/n}{L_s} \tag{1}$$

However, the symmetry will be disrupted with an OCF. For instance, Fig. 2(b) shows the waveforms when an OCF occurs on S_{21}, where the dashed line in faulty state denotes the pre-fault waveforms (the same as Figs. 4, 5, and 6). In the faulty interval, the current will be drawn from the neutral point o, and flow through D_1 instead of S_{21} due to the OCF on S_{21}, as shown in Fig. 3. As a result, the DC bias will appear on the inductor current due to the asymmetry, which will further increase the peak current. In addition, more charges will be drawn from the neutral point, and thus, the two capacitor voltages will be unbalanced. Similarly, the waveforms when an OCF occurs on the eight switches are shown in Fig. 4, and the FD approach is proposed based on the post-fault waveforms.

B. Proposed Fault Diagnosis Method

This letter analyzes the condition when an OCF occurs on a switch, while its anti-paralleled diode can operate normally. The proposed FD method is detailed as follows:

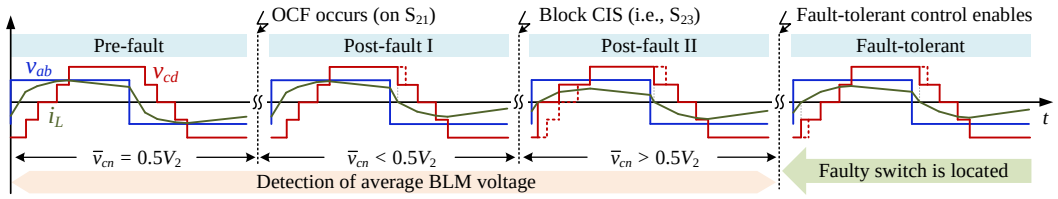

Fig. 6. Waveforms of the entire process for the proposed FD method.

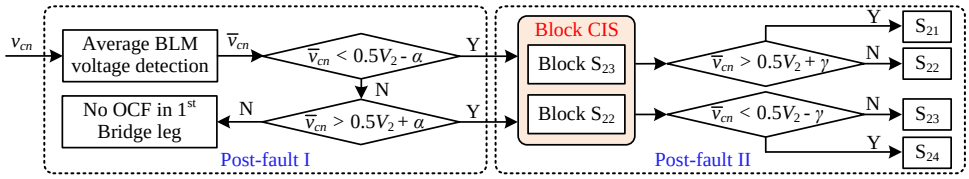

Fig. 7. Structure of the proposed FD method: the first bridge leg is taken as an example.

• *Step 1:* OCF identification by variation of BLM voltage

As shown in Fig. 2(a), the average BLM voltages v_{cn} and v_{dn} is $0.5V_2$ in a switching cycle in pre-fault state. However, when an OCF occurs on the first bridge leg, i.e., S_{21}, S_{22}, S_{23}, or S_{24}, the average BLM voltage $\overline{v}_{cn}$ will change. On the other hand, $\overline{v}_{dn}$ changes when an OCF occurs on the second leg, as shown in Fig. 4. Thus, it can be determined that an OCF occurs on a certain leg from the variation of $\overline{v}_{cn}$ or $\overline{v}_{dn}$.

• *Step 2:* Half leg location by average BLM voltage values

After Step 1, the two switches in the upper/lower bridge leg can be further located by the value of the average BLM voltage. As shown in Fig. 4, for the first bridge leg, when an OCF occurs on the upper leg (i.e., S_{21} or S_{22}), the average voltage $\overline{v}_{cn}$ is less than $0.5V_2$. Conversely, $\overline{v}_{cn}$ is higher than $0.5V_2$ when an OCF occurs on the lower leg (i.e., S_{23} or S_{24}). A similar condition applies also for the second bridge leg.

• *Step 3:* Specific faulty switch diagnosis by blocking CIS

When an OCF occurs on S_{22}, the post-fault waveform of v_{cd} can become symmetrical if the gate signal of S_{23} is blocked, and the average BLM voltage $\overline{v}_{cn}$ will return to $0.5V_2$, as shown in Fig. 5(a). Thus, S_{22} and S_{23} are defined as a CIS pair. On the other hand, if S_{21} is the faulty switch, the waveform of v_{cn} is not symmetrical and $\overline{v}_{cn}$ is higher than $0.5V_2$ after blocking S_{23}, as shown in Fig. 5(b). By doing so, the specific faulty switch can be identified by the value of $\overline{v}_{cn}$. With a similar analysis, the CIS S_{22} should be blocked if S_{23} and S_{24} are the possible faulty switches. Furthermore, when an OCF occurs on the second bridge leg, S_{26}/S_{27} is applied as the CIS to identify certain faulty switch.

Fig. 6 illustrates the entire process for the proposed FD method, including the pre-fault, post-fault I (after an OCF occurs), and post-fault II (after the CIS is blocked) states. It should be noted that with various modulation strategies, e.g., SPS control, TPS control, and five-level control, the NPC-based DAB converters exhibit similar post-fault characteristics on the variation of average midpoint voltages (which has been verified in [3]). Hence, the proposed FD method can be used to various modulation strategies. After the faulty switch is identified, a fault-tolerant control strategy, e.g., complementary-switch-blocking control [3], can be applied to suppress the negative OCF effects.

TABLE I
MAIN PARAMETERS USED IN THE EXPERIMENTS

Parameters	Values
Input/Output voltage V_1/V_2	120/300 V
Transformer turns ratio n	2
Series inductor L_s	100 μH
Switching frequency f_s	10 kHz
Thresholds α/γ	3/4 V

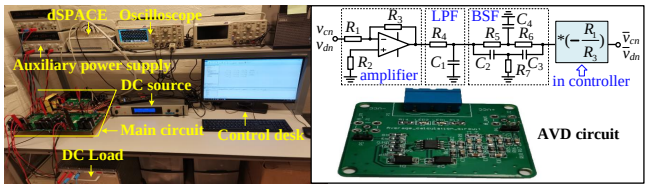

Fig. 8. Experimental prototype of DAB converter.

C. Implementation of Proposed Fault Diagnosis Method

With the above three steps, the implementation of the proposed FD approach can be shown as Fig. 7, where α is the threshold for detecting average BLM voltage in post-fault I, since the average voltage will be fluctuated around $0.5V_2$ in pre-fault state. The average voltage fluctuation is affected by various non-ideal factors, e.g., measurement noises, and parasitic parameters. Thus, α should be suitably chosen based on certain prototype to avoid false identification of OCF and improve the diagnosis accuracy. The determination of α has been detailed in [3]. In addition, γ is the other threshold during post-fault II, which can be determined in a similar way.

On the other hand, when an OCF occurs on the primary-side two-level bridge, the faulty switch can be identified directly by the average BLM voltages, while *Step 3* is not needed.

III. EXPERIMENTAL RESULTS

The proposed FD approach is validated by a prototype shown as Fig. 8, and the main parameters for experimental tests are given in Table I. The AVD circuit is also briefly shown in Fig. 8, which is composed of an amplifier (based on OPA2365), low-pass filter (LPF), and band-stop filter (BSF).

Fig. 9 shows the experimental waveforms after an OCF occurs on S_{21} and S_{22}, where it can be seen that the peak value of inductor current increases, especially when the OCF occurs on the inner switch S_{22} (from 18.5 A to 24 A). In addition, the

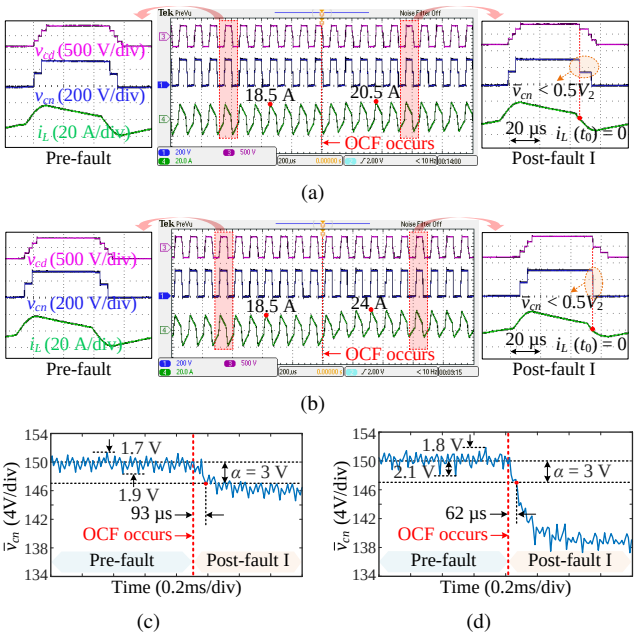

Fig. 9. Experimental results when the transferred power $P = 1.2$ kW, $D_2 = 0.16$, $D = 0.1$, and D_1 is regulated by closed-loop control: (a) and (b) are the experimental waveforms when an OCF occurs on S_{21} and S_{22}, respectively. (c) and (d) are the output results of the AVD circuit when an OCF occurs on S_{21} and S_{22}, respectively.

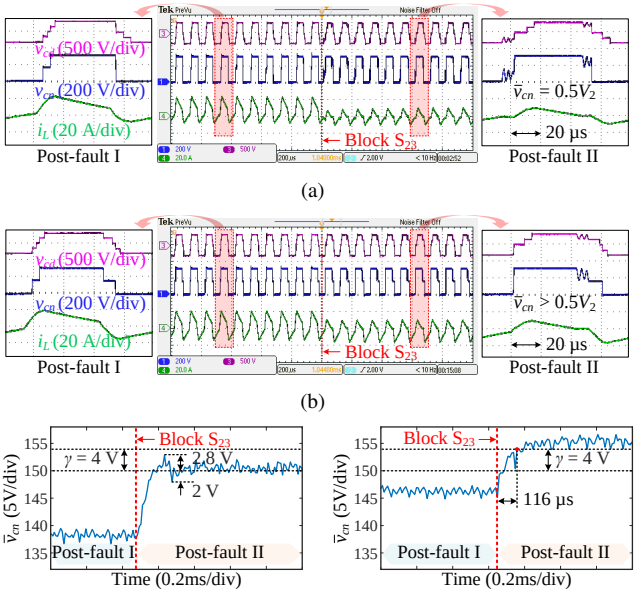

Fig. 10. Experimental results after blocking the CIS S_{23}: (a) and (b) are the experimental waveforms when an OCF occurs on S_{22} and S_{21}, respectively. (c) and (d) are the output results of the AVD circuit when an OCF occurs on S_{22} and S_{21}, respectively.

average BLM voltage $\overline{v}_{cn}$ is lower than $0.5V_2$ due to the faulty interval, as shown in the zoomed-in post-fault waveforms of Fig. 9(a) and (b). This characteristic is used in the first two steps of the proposed FD approach, which is detected by the AVD circuit. The output results of the AVD circuit are shown in Fig. 9(c) and (d), where it can be seen that the maximum noise on $\overline{v}_{cn}$ in pre-fault state is around ± 2 V. After leaving certain margin for avoiding false OCF diagnosis, the threshold α during post-fault I is set as 3 V. When the OCF occurs on S_{21} and S_{22}, the average BLM voltage $\overline{v}_{cn}$ decreases, and will

TABLE II
COMPARISON BETWEEN TRADITIONAL AND PROPOSED FD METHODS

FD Method	Diagnostic Period	Additional Hardware
FD Method in [3]	$< 2T_s$①	4∗voltage-sensor-based circuit
Proposed FD method	$< 4T_s$	4∗AVD circuit

①: $T_s = 2T_{hs}$ is a switching cycle

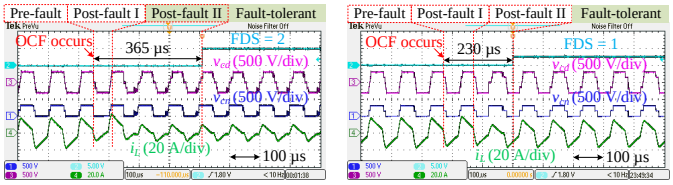

Fig. 11. Experimental results for the extire process of the proposed FD method when an OCF occurs on: (a) S_{22}, and (b) S_{21}.

exceed the threshold α after 93 μs and 62 μs, respectively. The threshold γ in post-fault II can be determined in a similar way. As shown in Fig. 10(a) and (c), for the condition when the OCF occurs on S_{22} and the CIS S_{23} is blocked, the waveform of v_{cd} becomes symmetrical, and $\overline{v}_{cn}$ increases from post-fault I, and will fluctuate around $0.5V_2$. It can be seen from Fig. 10(c) that the maximum noise is 2.8 V, and thus, the threshold γ is chosen as 4 V. On the other hand, if the OCF occurs on S_{21}, the waveform of v_{cd} is still asymmetrical, and $\overline{v}_{cn}$ will exceed the threshold γ after 116 μs, as shown in Fig. 10(b) and (d). In the proposed FD method, the average BLM voltage is monitored in three series switching cycles after the CIS is blocked. If $\overline{v}_{cn}$ exceeds the threshold γ in this duration, S_{21} is diagnosed as the faulty switch. Otherwise, the OCF is identified to occur on S_{22}.

Fig. 11 illustrates the entire process of the proposed FD approach, where it can be seen that the fault diagnostic sign (FDS) will turn on within four switching periods, where FDS = 1 and 2 indicate that the OCF occurs on S_{21} and S_{22}, respectively. Furthermore, the diagnosis for the inner switch S_{22} will be slower than that of the outer switch S_{21}, as the diagnosis for S_{22} during post-fault II needs to last for three switching periods. After the FDS turns on and the faulty switch is identified, a fault-tolerant control based on complementary-switch-blocking method, proposed in [3], is applied to bring the converter back to safe operation. If the OCF occurs on S_{22}, the operation will be transferred to fault-tolerant state when S_{23} is blocked, i.e., from post-fault II. This is because S_{23} is the complementary switch of S_{22} (the details can be seen in [3]), which means the waveforms of v_{cd} and i_L can become symmetrical, and the negative OCF effects (e.g., DC bias and current overshoots) can be diminished after blocking S_{23}, as shown in Fig. 11(a). Therefore, although the diagnostic period for inner switch S_{22} increases, the DAB converter can enter fault-tolerant state before it can be diagnosed (i.e., FDS turns on), and thus, the increased diagnostic time will not affect the safe operation of DAB converter. On the other hand, when the OCF occurs on S_{21}, the CIS S_{23} should return to normal working condition. Instead, its complementary switch S_{24} should be blocked, and then, the converter can be transferred to fault-tolerant state, as shown in Fig. 11(b).

A comparison between the proposed FD method and the

sensor-based method in [3] is shown in Table II. Four additional voltage sensors are applied to the traditional FD method, which increases the hardware costs significantly compared to the proposed FD method, e.g., the unit price of the voltage sensor LV25-P used in [3] is around 75 €, while that of the operational amplifier is much lower. In addition, although the diagnostic time increases from two to four switching cycles with the proposed method, the OCF effects will not threaten the safe operation of DAB converter in such a short period.

IV. Conclusion

This letter has proposed a generic sensorless FD method for the NPC-based DAB converters, which is suitable for various modulation strategies. In this method, the average BLM voltages are utilized to determine two possible faulty switches in a same upper/lower bridge leg by an AVD circuit. Subsequently, specific faulty switch can be identified by the average BLM voltages after blocking certain CIS. The control structure of this FD method is simple as only the average BLM voltages are applied as diagnostic signal. Experimental results show that the diagnostic period increases slightly with the proposed FD approach compared to traditional sensor-based method. However, this has no significant impact on the DAB converters, as the faulty switch can still be identified within four switching cycles. Conversely, the hardware costs can be reduced significantly by the proposed FD method. Furthermore, the proposed FD method can provide references to the fault-related analysis in the future. For instance, the CIS is blocked to differentiate the inner and outer switches, which indicates that the topology symmetry of the NPC bridge can be utilized to distinguish certain similar faulty conditions.

References

[1] P. Liu, C. Chen, and S. Duan, "An Optimized Modulation Strategy for the Three-Level DAB Converter With Five Control Degrees of Freedom," *IEEE Trans. Ind. Electron*., vol. 67, no. 1, pp. 254-264, Jan. 2020.

[2] C. Song, A. Sangwongwanich, Y. Yang, Y. Pan, and F. Blaabjerg, "Analysis and Optimal Modulation for 2/3-Level DAB Converters to Minimize Current Stress With Five-Level Control," *IEEE Trans. Power Electron*., vol. 38, no. 4, pp. 4596-4612, Apr. 2023.

[3] C. Song, A. Sangwongwanich, Y. Yang, and F. Blaabjerg, "Open-Circuit Fault Diagnosis and Tolerant Control for 2/3-Level DAB Converters," *IEEE Trans. Power Electron*., vol. 38, no. 4, pp. 5392-5410, Apr. 2023.

[4] N. Zhao, J. Liu, Y. Shi, J. Yang, J. Zhang, and X. You, "Mode Analysis and Fault-Tolerant Method of Open-Circuit Fault for a Dual Active-Bridge DC-DC Converter," *IEEE Trans. Ind. Electron*., vol. 67, no. 8, pp. 6916-6926, Aug. 2020.

[5] S. K. Rastogi, S. S. Shah, B. N. Singh, and S. Bhattacharya, "Mode Analysis, Transformer Saturation, and Fault Diagnosis Technique for an Open-Circuit Fault in a Three-Phase DAB Converter," *IEEE Trans. Power Electron*., vol. 38, no. 6, pp. 7644-7660, Jun. 2023.

[6] M. Puthiyapurayil, M. Ramees, M. Nasirudeen, Y. Saywan, M. Ahmad, and H. Malik. "A Review of Open-Circuit Switch Fault Diagnostic Methods for Neutral Point Clamped Inverter," *Electronics*. 2022; 11(19):3169.

[7] M. Zhang, Z. Zhang, Z. Li, H. Chen, and D. Zhou, "A Unified Open-Circuit-Fault Diagnosis Method for Three-Level Neutral-Point-Clamped Power Converters," *IEEE Trans. Power Electron*., vol. 38, no. 3, pp. 3834-3846, Mar. 2023.

[8] X. Wei, H. Wang, A. Luo, Z. He, X. Zhu, R. Sun, and X. Chen, "Parallel Open-Circuit Fault Diagnosis Method of a Cascaded Full-Bridge NPC Inverter With Model Predictive Control," *IEEE Trans. Ind. Electron*., vol. 68, no. 10, pp. 10180-10192, Oct. 2021.

[9] B. Shi, B. Zhou, Y. Zhu, X. Qin, J. Lei, and N. Han, "Open-Circuit Fault Analysis and Diagnosis for Indirect Matrix Converter," *IEEE J. Emerg. Sel. Topics Power Electron*., vol. 6, no. 2, pp. 770-781, Jun. 2018.

[10] D. Xie, and X. Ge, "Open-Circuit Fault Diagnosis of Dual Active Bridge DC-DC Converter Based on Residual Analysis," in *Proc. PEAC*, Shenzhen, China, 2018, pp. 1-6.

[11] J. Li, H. Wen, H. Shi, and W. Liu, "Fault Diagnosis of Isolated Bidirectional DC/DC Converter with Triple Phase-Shift Control," in *Proc. PEDG*, Xi'an, 2019, pp. 279-282.

[12] S. S. Khan and H. Wen, "Universal Sensorless Open-Circuit Fault Detection and Isolation Method of Dual-Active-Bridge Converters With Low-Cost Diagnostic Circuit," *IEEE Trans. Power Electron*., vol. 37, no. 11, pp. 13652-13667, Nov. 2022.

[13] H. Shi, H. Wen, and J. Li, "Fault Analysis and Fault-Tolerant Method of Dual Active Bridge Converter under Triple Phase Shift Control," in *Proc. ECCE-Asia*, Busan, Korea, 2019, pp. 1121-1127.

[14] H. Wen, J. Li, H. Shi, Y. Hu, and Y. Yang, "Fault Diagnosis and Tolerant Control of Dual-Active-Bridge Converter with Triple-Phase-Shift Control for Bidirectional EV Charging Systems," *IEEE Trans. Transportation Electrification*., vol. 7, no. 1, pp. 287-303, Mar. 2021.

[15] M. Zheng, H. Wen, H. Shi, Y. Hu, Y. Yang, and Y. Wang, "Open-Circuit Fault Diagnosis of Dual Active Bridge DC-DC Converter With Extended-Phase-Shift Control," *IEEE Access*., vol. 7, pp. 23752-23765, 2019.

[16] J. Wu, H. Wang, M. Ma, Q. Chen, and J. Liang, "Mode Analysis and Fault-Tolerant Method of Open-Circuit Fault for a Three-Level Dual Active Bridge DC-DC Converter," *Microelectronics Reliability*, Volume 150, 2023.